Glass transition and bond-orientational symmetries in rapidly supercooled one-component plasmas: Monte Carlo simulation study

Shuji Ogata and Setsuo Ichimaru
Department of Physics, University of Tokyo, 7-3-1 Hongo, Bunkyo-ku, Tokyo 113, Japan
(Received 1 August 1988)

Through Monte Carlo simulations of rapidly quenched one-component plasmas, we investigate microscopically the dynamic evolutions of local and extended bond-orientational symmetries in supercooled states and show that the resulting states are the Coulomb glasses. The glass states are characterized by random polycrystalline structures with long-range bond-orientational order; in these states the particles are virtually locked around their equilibrium positions. The inverse temperature at the glass transition is found between 200 and 300 in units of the average Coulomb energy. The polycrystalline structures of the resulting glasses depend sensitively on how the rapid quench is applied. Physical problems specific to the Coulombic systems are discussed.

I. INTRODUCTION

Various attempts have been made to investigate metastability of supercooled fluids and processes of solidification (i.e., crystallization and glass transition) through molecular-dynamics (MD) and Monte Carlo (MC) simulation methods in systems such as the hard spheres,[1,2] Lennard-Jones,[3,4] and inverse power[5,6] systems. Those simple fluids, if quenched rapidly, have been found to form glasses and exhibit many properties similar to those commonly observed in complex glassy systems.

The classical one-component plasma[7] (OCP) is a system consisting of charged particles of a single species, with electric charge Ze, number density n, and temperature T, embedded in a uniform neutralizing background of opposite charges. The state of such a system can be characterized by the Coulomb coupling constant

$$\Gamma=(Ze)^2/ak_BT\ , \tag{1}$$

the inverse temperature in units of the average Coulomb energy, where

$$a=(4\pi n/3)^{-1/3} \tag{2}$$

is the ion-sphere radius.

The OCP differs from the simple fluids mentioned above in various ways: We note in particular that the Coulomb force is a long-range one and that no volume fluctuations exist owing to the presence of the uniform background of neutralizing charges. It has been predicted[8,9] that the OCP undergoes a first-order freezing transition (i.e., a Wigner transition) to the bcc-lattice phase at $\Gamma_m=178$–180. An outstanding problem associated with such a transition is an investigation in evolution of microscopic structures and bond-orientational symmetries as the plasma is supercooled below the transition temperature, $\Gamma>\Gamma_m$.

In the computer-simulation studies of the phase evolution in ordinary substances, one resorts to the MD methods at constant temperature and pressure;[10,11] the scheme of microcanonical MD simulation needs adequate modifications, however, to accommodate such conditions. The MC methods, on the other hand, can naturally incorporate isothermal and/or isobaric conditions with the appropriate energy and/or volume fluctuations. The situation is simplified further in the cases of the OCP since the volume fluctuations vanish automatically.

The major shortcoming of the MC method in the phase-evolution study is an apparent lack of the "time" concept. To find a way to circumvent such a shortcoming, we performed several series of MC runs for strongly coupled ($\Gamma\geq 80$) OCP's both in the fluid and in the crystalline states, and thereby analyzed the microscopic features of the MC trajectories as functions of the sequential number c of the MC configurations measured in units of a million configurations. Detailed investigations[12] have revealed that the MC particles behave as if they are trapped in the potential dimples of ion spheres[7] in the small c/N regime ($c/N<10^{-4}$), where N is the number of the MC particles; in the large c/N regime ($c/N>10^{-3}$), they perform diffusive motions in the fluid simulations, and remain localized around the lattice sites in the crystalline simulations. We then carried out a MC simulation analysis of Brownian particles in a dimple of the ion-sphere potential, and thereby found a correspondence between c and "MC time" t:

$$c/N=[(23.0\pm 0.8)\times 10^{-6}]2\omega_p t/\sqrt{3}\pi\ , \tag{3}$$

where ω_p is the plasma frequency. Application of this correspondence in the large c regime leads to an estimate of the diffusion coefficient in the fluid regime, which agrees well with the one evaluated independently through the MD simulation method.[13]

In this paper we thus investigate the dynamic evolutions of microscopic structures and bond-orientational symmetries in the supercooled OCP's through the MC simulation method. In Sec. II we institute four cases of rapid quenches into supercooled states starting with an equilibrated fluid state at $\Gamma=160$; those are simulated by four distinct runs of the MC simulations. In Sec. III we define and introduce various parameters and functions

describing the local and extended bond-orientational symmetries. In Sec. IV we investigate the microscopic correlations and bond-orientational symmetries in a fluid simulation at $\Gamma=160$ and in a bcc-lattice simulation at $\Gamma=400$; those provide frames of reference for comparison with the rapid-quench simulations. Section V contains the main results of the present MC simulation study in the four cases of the rapidly supercooled OCP's; the microscopic structures of the glass states are investigated in detail. Concluding remarks are given in Sec. VI.

II. QUENCHING PROCESSES

For the MC simulations of infinite systems, one finds it desirable to increase the number N of the particles in the MC cell under the periodic boundary conditions, so that the effects of the boundary conditions may be minimized. The "MC elapsed time"[12] is then proportional to c/N and thus decreases with N at the same c. To find a way to compromise between those two opposing effects of N, we note that the computed values of the excess internal energy have remained almost constant within error bars for $N=432$, 686, and 1024 in the earlier study.[9] We hence choose the smallest number 432, which corresponds to the side length $L\simeq 12a$ of the MC cell.

Four distinct runs of the MC simulations are performed to study evolution of microscopic correlations in rapidly quenched OCP's, starting with an equilibrated fluid state at $\Gamma=160$: (A) an application of a "sudden quench" to $\Gamma=400$ at $c=0$; (B) an application of a "gradual quench" stepwise with $\Delta\Gamma=10$ from $\Gamma=160$ at $c=0$ to $\Gamma=400$ at $c=23$; (C) a sudden quench to $\Gamma=300$ at $c=0$; and (D) a sudden quench to $\Gamma=200$ at $c=0$. The phase evolutions have been subsequently monitored up to $c=80$ for (A), (B), and (C), and up to $c=30$ for (D).

Since we adopt

$$P(r)=(2\Gamma/\pi)^{1/2}\Gamma(r/a)^2\exp[-\Gamma(r/a)^2/2] \tag{4}$$

as the probability of random displacements $\mathbf{r}$ of the MC particles,[12] we find the correspondence of the MC time as

$$\omega_p t=2.7\times 10^2 c \tag{5}$$

in the present cases of simulation.

III. BOND-ORIENTATIONAL ORDER PARAMETERS

The local bond-orientational symmetries are studied in terms of the spherical harmonics, $Q_{lm}(\mathbf{r})=Y_{lm}(\theta(\mathbf{r}),\phi(\mathbf{r}))$, where $\theta(\mathbf{r})$ and $\phi(\mathbf{r})$ are the polar angles of the bond joining two neighboring particles; the particle positions are averaged over a sequence of 0.3 in order to reduce thermal fluctuations. Following Steinhardt *et al.*[14] and Nosé and Yonezawa,[15] we introduce the following bond-orientational parameters, which are rotationally invariant combinations of the second and the third order:

$$Q_l=\left[\frac{4\pi}{2l+1}\sum_{|m|\le l}|\langle Q_{lm}(\mathbf{r})\rangle|^2\right]^{1/2}, \tag{6}$$

$$W_l=\sum_m \begin{pmatrix} l & l & l \\ m_1 & m_2 & m_3 \end{pmatrix} \frac{\bar{Q}_{lm_1}\bar{Q}_{lm_2}\bar{Q}_{lm_3}}{\left[\sum_{|m|\le l}|\bar{Q}_{lm}|^2\right]^{3/2}}. \tag{7}$$

The coefficients in Eq. (7) are the Wigner $3j$ symbols, whose summation is carried out with $m_1+m_2+m_3=0$. Unless specified otherwise, we define a bond as that between those particles whose separation is less than $2.3a$, approximately the distance at which the radial distribution function $g(r)$ takes on its first minimum.

The average $\bar{Q}_{lm}$ in Eq. (7) is carried out with regard to all of such bonds around a given particle; $\langle\ \rangle$ in Eq. (6) means analogous average with respect to such bonds over all the MC particles. The number of neighboring particles within the radius of $2.3a$, that is, "coordination number N_c" is 12 for the *fcc, hcp,* and *icosahedral* clusters (close packing structures); it is 14 for the *bcc* clusters.

The rotationally invariant quantities, Q_l and W_l, play the key part in cluster "shape spectroscopy" in liquids and glasses.[14] Q_l takes on a first nonvanishing value (other than Q_0) for $l=4$ in samples with cubic symmetry and for $l=6$ in icosahedrally oriented systems. The ratios W_l in particular are a sensitive measure of the different orientational symmetries. We list in Table I the values of Q_4, Q_6, W_4, and W_6 for four types of the clusters mentioned above.

The quantities Q_4 and Q_6 are defined in terms of averages over *all* the particles in the MC cell; hence, they can describe bond-orientational symmetries in the entire MC cell. In Table I we observe that the values of Q_4 differ significantly from each other among the four types of clusters, while the values of Q_6 remain almost the same. The quantity Q_4 is thus more useful than Q_6 in distinguishing between different bond-orientational symmetries in the MC cell.

The quantities W_4 and W_6, on the other hand, are defined in terms of averages over bonds around an *individual* MC particles. In Table I we find that the local bond-orientational symmetries around a particle can be discerned through its location on the two-dimensional (W_4, W_6) map. (See Sec. V for details.) We remark that W_4 is not a well-defined quantity for the icosahedron

TABLE I. Values of Q_4, Q_6, W_4, and W_6 calculated with $N_c=12$ for the *fcc*, *hcp*, and *icosahedral* clusters and with $N_c=14$ for the *bcc* clusters.

	Q_4	Q_6	W_4	W_6
fcc	0.1909	0.5745	−0.1593	−0.0132
hcp	0.0972	0.4848	0.1341	−0.0124
icosahedral	0	0.6633		−0.1698
bcc	0.0364	0.5107	0.1593	0.0132

since $Q_4=0$; W_6 is negative and its magnitude is distinctly larger by an order of magnitude than those for the other three clusters.

The extended bond-orientational symmetries are studied in terms of the correlation functions

$$G_l(r)=\frac{4\pi}{(2l+1)G_0(r)}\sum_{|m|\le l}\langle Q_{lm}(\mathbf{r})Q_{l-m}(\mathbf{0})\rangle \qquad (8)$$

where $G_0(r)=4\pi\langle Q_{00}(\mathbf{r})Q_{00}(\mathbf{0})\rangle$.

IV. MC SIMULATIONS FOR FLUID AND LATTICE OCP'S

In order to establish frames of reference whereby we may study comparatively the degrees of local bond-orientational symmetries developed in the quenched OCP's, we carry out a fluid simulation at $\Gamma=160$ and a bcc-lattice simulation at $\Gamma=400$, and measure the correlation functions and the bond-orientational order parameters in those simulations.

The radial distribution function in the fluid case, shown in Fig. 1(a), is a smooth function of r, while $g(r)$ in the bcc-lattice case exhibits prominent peaks reflecting the bcc crystalline structures. For the fluid case, $Q_4\simeq 0.01$ and $Q_6\simeq 0.03$; for the bcc-lattice case, $Q_4\simeq 0.04$ and $Q_6\simeq 0.5$, indicating the existence of bond-orientational symmetries over the entire MC cell. Fractional numbers of the particles with $N_c=12$, 13, and 14 are 0.3, 0.4, and 0.2, respectively, for the fluid phase; fractions with $N_c\le 11$ and $N_c\ge 15$ are negligible. In the bcc-lattice case all the particles have $N_c=14$.

Particles with $N_c=12$ and 14 are singled out and are plotted on the two-dimensional (W_4,W_6) maps with open and solid circles, respectively: Fig. 2(a) for the fluid case and Fig. 2(b) for the bcc-lattice case. In those figures, diamond markers are entered for the fcc, hcp, icosahedral, and bcc clusters according to the values of W_4 and W_6 in Table I (the value of W_4 for the icosahedron is arbitrarily set to zero in the figures). In the fluid case, particles with $N_c=12$ and 14 are scattered widely on the map, with more particles located in the lower half, $W_6<0$. In the bcc-lattice case, almost 90% of the particles with $N_c=14$ are found in the first quadrant. Due to thermal fluctuations, the particle locations depart from the diamond marker of the exact bcc cluster, and some particles are found even in the second quadrant.

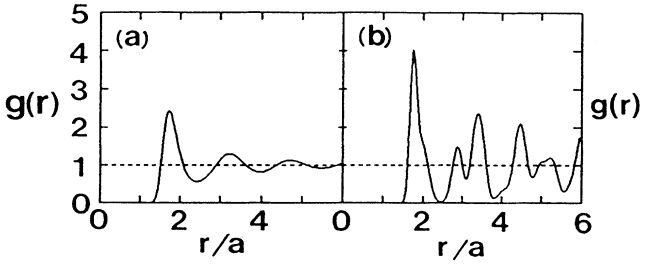

FIG. 1. The radial distribution functions in the fluid and bcc-lattice OCP's: (a) is the fluid simulation at $\Gamma=160$; (b) the bcc-lattice simulation at $\Gamma=400$.

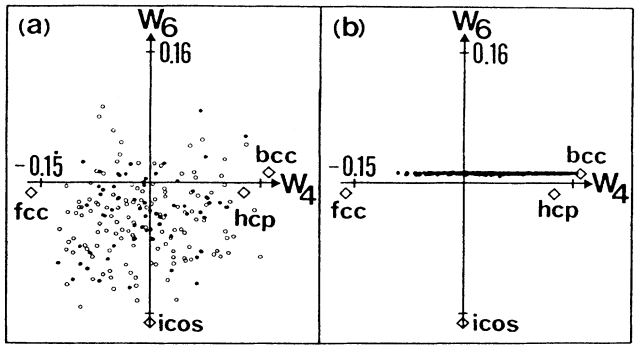

FIG. 2. Two-dimensional (W_4,W_6) maps in the fluid and bcc-lattice OCP's: (a) is the fluid simulation at $\Gamma=160$; (b) the bcc-lattice simulation at $\Gamma=400$. Open circles indicate those particles with $N_c=12$; solid circles, $N_c=14$. Diamond markers depict the W_4 and W_6 values in Table I for the fcc, hcp, icosahedral, and bcc clusters; for the icosahedron, we set $W_4=0$ here.

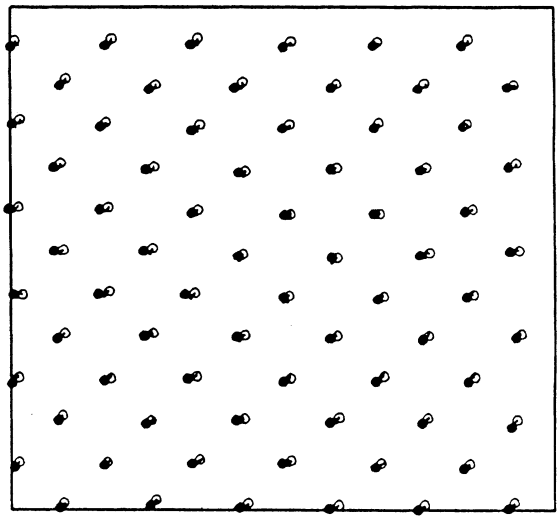

FIG. 3. Two-dimensional (x,y) mappings of the real-space trajectories of the MC particles located within thickness $\Delta z=2a$ in the bcc-lattice simulation at $\Gamma=400$. Particles moves from the open circles to the solid circles during an interval of eight.

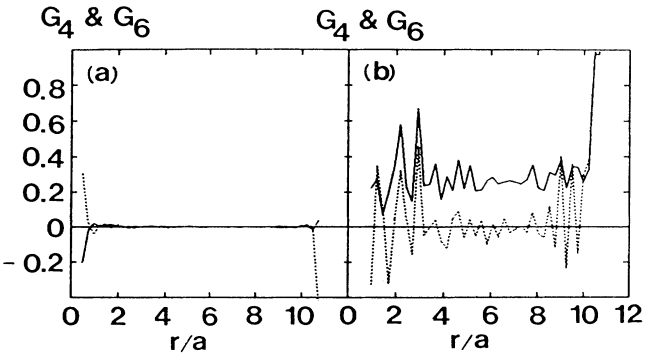

FIG. 4. Correlation functions $G_4(r)$ (dotted lines) and $G_6(r)$ (solid lines) in the fluid and bcc-lattice OCP's: (a) is the fluid simulation at $\Gamma=160$; (b) the bcc-lattice simulation at $\Gamma=400$.

Two-dimensional (x,y) mappings of the real-space trajectories of the MC particles located within thickness $\Delta z = 2a$ are shown in Fig. 3 for the bcc-lattice case; the particle positions are averaged over 0.3 in every million configurations and are followed during an interval of eight. The initial positions of the MC particles are designated by the open cirlces and the end positions by the solid circles. Since the center of mass is not fixed in MC simulations, we observe here that a uniform displacement of the entire system is involved even in the bcc-lattice simulation.

Figure 4(a) indicates that $G_4(r) \simeq 0$ and $G_6(r) \simeq 0$ over the MC-cell volume in the fluid case; no extended bond-orientational symmetries are observed. In the bcc lattice of Fig. 4(b), we observe $G_4(r) \simeq 0$ and $G_6(r) \simeq 0.25$ over the MC-cell volume, indicating the existence of bond-orientational symmetries. Since $G_4(r) \simeq 0$ in both phases, we may conclude that $G_4(r)$ is not an appropriate quantity for an investigation of the extended bond-orientational symmetries.

V. MC SIMULATIONS OF RAPIDLY QUENCHED OCP's

We investigate sequential developments of the following quantities in the rapidly quenched OCP's for the MC runs (A)–(D) of Sec. II: The excess internal energy U (see, e.g., Ref. 7); $g(r)$; N_c; Q_4 and Q_6; particle distributions on the two-dimensional (W_4, W_6) maps; two-dimensional (x,y) mappings of the real-space trajectories of those MC particles located within thickness of $\Delta z = 2a$, over an interval of eight; $G_4(r)$ and $G_6(r)$. Those are compared also with the results of the fluid and bcc-lattice simulations described in the preceding section.

Figure 5 summarizes the evolution of the normalized excess internal energies, $u = U/Nk_BT$, in the four quenching processes. In the figure we also depict the values (the dashed lines) predicted from the extensions of the fluid internal-energy formulas[8]

$$u = -0.897\,744\Gamma + 0.950\,43\Gamma^{1/4} + 0.189\,56\Gamma^{-1/4} - 0.814\,87 \quad (9)$$

and[9]

$$u = -0.898\,004\Gamma + 0.967\,86\Gamma^{1/4} + 0.220\,703\Gamma^{-1/4} - 0.860\,97\ , \quad (10)$$

and the bcc-lattice values (the dot-dashed lines) according to the formula[8]

$$u = -0.895\,929\Gamma + 1.5 + 3225\Gamma^{-2}\ . \quad (11)$$

We find in Fig. 5 that after the rapid quenches (A), (B), and (C), the excess internal energies relax to metastable levels for $c \geq 24$–29, which lie distinctly below the extensions of the fluid internal-energy formulas (9) and (10), and which stay somewhat above the bcc-lattice values (11). Specifically in the quench (A), after a sudden initial decrease, u stays around the levels of Eqs. (9) and (10) for $2 \leq c \leq 7$, decreases steeply at $c \simeq 13$, and relaxes to the metastable level for $c \geq 28$. Analogously in the quench (C), u stays around the extended fluid values for $1 \leq c \leq 6$, decreases steeply at $c \simeq 8$, finds itself in a "plateau" state at $9 \leq c \leq 23$, and relaxes to the metastable level for $c \geq 24$. We proceed to investigate the sequential evolutions of the correlation functions and the bond-orientational symmetries in the four cases of rapid quenches, in reference to Fig. 5.

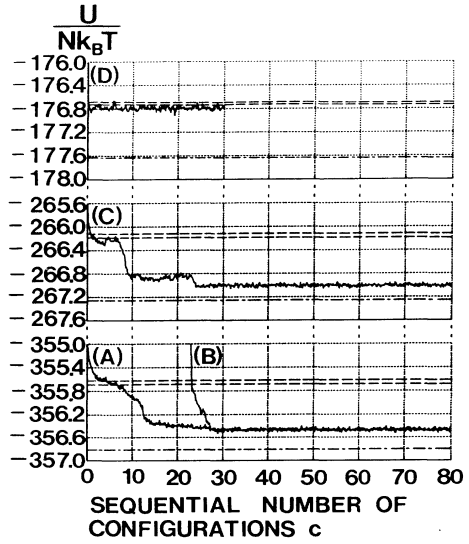

FIG. 5. Evolution of the normalized excess internal energies for the MC simulation runs (A), (B), (C), and (D), explained in the text. The dashed lines indicate the levels predicted from extensions of the fluid internal-energy formulas [top: Eq. (9); bottom: Eq. (10)] at the Γ values in the metastable states after quenches; the dot-dashed lines, the bcc crystalline levels, Eq. (11).

A. Sudden quench to $\Gamma = 400$

The radial distribution functions $g(r)$ at various stages of the sequential evolution are plotted in Figs. 6: At $c = 7$, $g(r)$ is a smooth function of r and resembles the

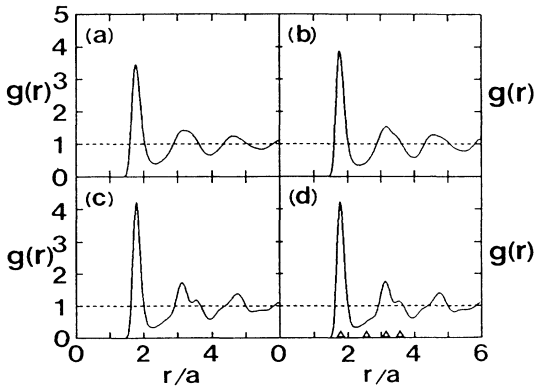

FIG. 6. The radial distribution functions: (a) at $c = 7$, (b) at $c = 15$, (c) at $c = 40$, and (d) at $c = 80$, for the MC simulation run of the sudden quench (A) to $\Gamma = 400$. The triangular markers depict the positions of nearest-neighbor particles in the fcc-hcp structures.

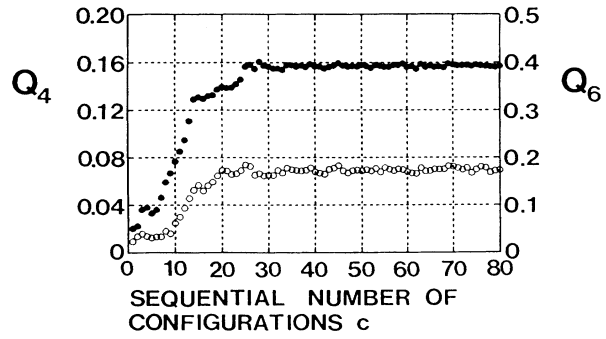

FIG. 7. Evolution of the Q_4 and Q_6 values for the MC simulation run of the sudden quench (A) to $\Gamma=400$. Open circles correspond to Q_4 values; solid circles, Q_6 values.

fluid case in Fig. 1; at $c=15$, the second peak of $g(r)$ acquires a shoulder; at $c=40$, the second peak is split into two peaks, which correspond to peaks for the fcc or hcp lattice; at $c=80$, no significant changes from the case at $c=40$ can be detected.

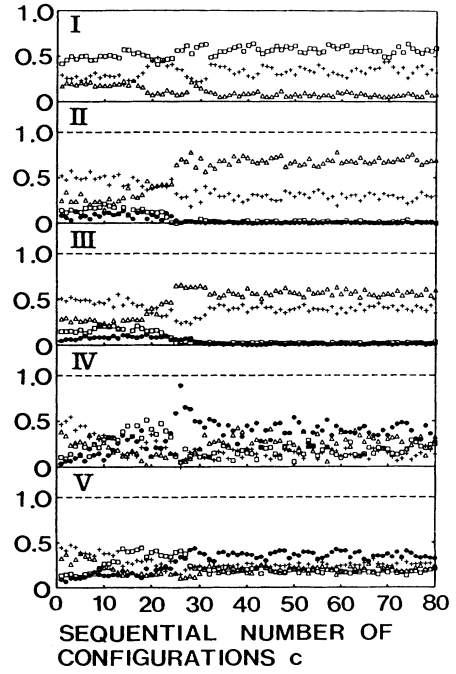

FIG. 8. Evolution of fractional numbers of various clusters for the sudden quench (A) to $\Gamma=400$. I, crosses, the clusters with $N_c=12$; square $N_c=13$; and triangles, $N_c=14$. II, for the clusters with $N_c=12$, solid circles indicate those on the first quadrant in the (W_4, W_6) map; squares, the second quadrant; crosses, the third quadrant (identified as "fcc"; triangles, the fourth quadrant (identified as "hcp"). III, Same as II, but for the clusters with $N_c=13$ reassembled to "$N_c=12$." IV, for the clusters with $N_c=14$, solid circles indicate those on the first quadrant (identified as 'bcc"); squares, the second quadrant; crosses, the third quadrant; triangles, the fourth quadrant. V, same as IV, but for the clusters with $N_c=13$ reassembled to "$N_c=14$."

Sequential evolutions of Q_4 and Q_6 are shown in Fig. 7, and are observed to have an intimate connection with those of the excess internal energies (Fig. 5). For $2\leq c\leq 7$, $Q_4\simeq 0.015$ and $Q_6\simeq 0.1$; for $9\leq c\leq 13$, they increase monotonically to $Q_4\simeq 0.06$ and $Q_6\simeq 0.3$; at $c\simeq 24$, $Q_4\simeq 0.07$ and Q_6 increases stepwise to 0.4 and remains constant thereafter. For comparison we recall $Q_4\simeq 0.01$ and $Q_6\simeq 0.03$ in the fluid case at $\Gamma=160$. The observed final values of Q_4 leads us to conclude that a bond-orientational symmetry has been developed over the entire MC cell in the metastable state.

Fractional numbers of the particles with $N_c=12$, 13, and 14 in the metastable state ($c\geq 30$) relax to 0.35, 0.55, and 0.10, respectively, as shown in Fig. 8I. The fraction with $N_c=14$ is somewhat smaller, while that with $N_c=13$ is somewhat larger, than those in the fluid case at $\Gamma=160$.

Particles with $N_c=12$ and 14 are plotted on the (W_4, W_6) maps in Fig. 9, in the same way as in Fig. 2: At $c=7$, particles with $N_c=12$ and 14 are widely scattered as in the fluid case of Fig. 2(a); at $c=15$, particle distributions with $N_c=12$ and 14 shrink toward the abscissa ($W_6=0$); at $c=40$, particles with $N_c=12$ are gathered toward the fcc and hcp markers; the state at $c=80$ appears much the same as that at $c=40$, both being in the metastable state.

Particles are divided into four groups according to the locations on the quadrants of the (W_4, W_6) plane. Since the majority of the particles have $N_c=13$, we calculate their W_4 and W_6 also by taking 12 and 14 nearest neighbors; we then classify those reassembled particles according to the signs of W_4 and W_6. Sequential evolutions of the fractional numbers in those four groups are plotted in Figs. 8II–V. No significant differences are observed be-

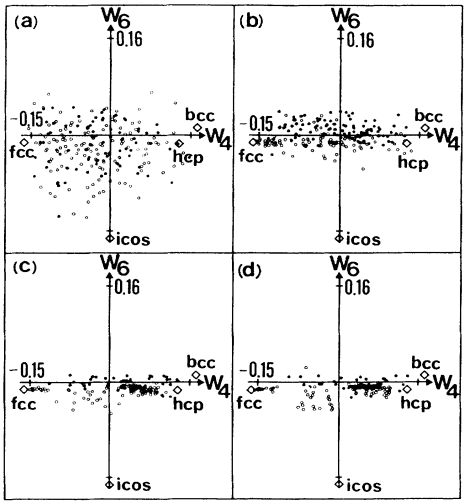

FIG. 9. Two-dimensional (W_4, W_6) maps: (a) at $c=7$; (b) at $c=15$; (c) at $c=40$; and (d) at $c=80$, for the MC run of the sudden quench (A) to $\Gamma=400$. Open circles represent those particles with $N_c=12$; solid circles, $N_c=14$. The diamond markers correspond to the fcc, hcp, icosahedral, and bcc clusters in Table I (for icosahedron, we set $W_4=0$ here).

tween the behaviors of the original particles with $N_c=12$ or 14 and of those $N_c=13$ particles reassembled to "$N_c=12$ or 14." At the onset of the metastable state ($c\simeq 28$), we clearly observe turning overs of the fractional numbers so that the "bcc" particles (in the first quadrant) become the largest in number among the "$N_c=14$" particles, while the "hcp" (in the fourth quadrant) and "fcc" (in the third quadrant) particles are the major constituents in the "$N_c=12$" particles.

To see whether the metastable state belongs to a fluid or a solid state, a two-dimensional (x,y) mapping of the MC-particle positions within thickness $\Delta z=2a$ is shown in Fig. 10 (top) from $c=70$ (open circles) to $c=78$ (solid circles). Contrary to the bcc-lattice case in Fig. 3, a long-range translational order is apparently destroyed. Analogous to the bcc-lattice case, no diffusive motions of the particles are observed, and a translational motion of the particles as a whole remains (due to the nature of MC simulations). We may therefore conclude that the metastable state realized in the rapid quench (A) for $c\geq 28$ is a solid state without a long-range translational order, implying a glass state.

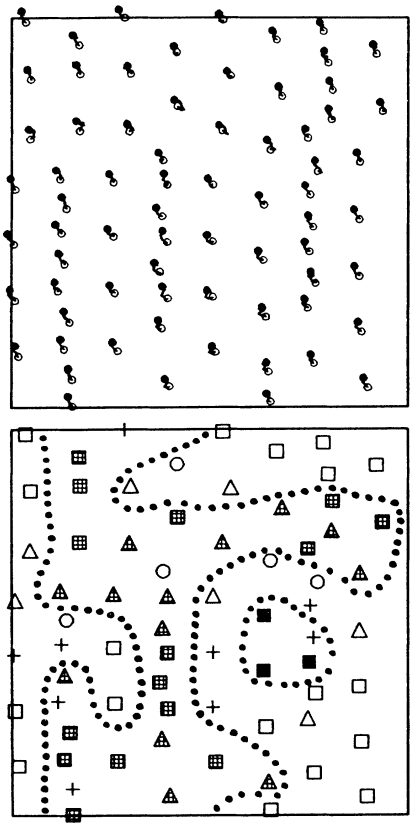

FIG. 10. Top: Two-dimensional (x,y) mapping of the MC particle positions within thickness $\Delta z=2a$ in the metastable state for the MC run of the sudden quench (A) to $\Gamma=400$. Particles move from the open circles at $c=70$ to the solid circles at $c=78$. Bottom: Local bond-orientational symmetry associated with the particles in the figure (top). See the text for the meaning of the markers. Domain boundaries, drawn by dotted curves, are only for a guide to the eye.

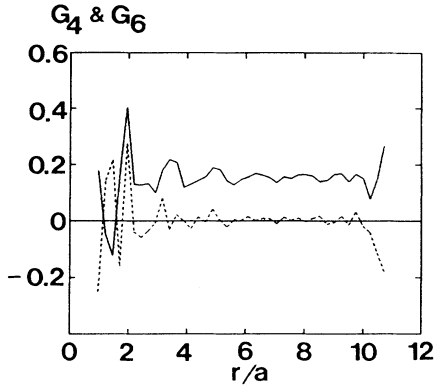

FIG. 11. Correlation functions $G_4(r)$ (dotted line) and $G_6(r)$ (solid line) at $c=60$ in the MC simulation run of the sudden quench (A) to $\Gamma=400$.

To investigate the local bond-orientational symmetries associated with those interlocked particles in Fig. 10 (top), we identify each particle in terms of its signature characterizing the bond-orientational symmetry in Fig. 10 (bottom). Thus, a particle with $N_c=12$ is identified as "fcc" (a shaded square) if it is located in the third quadrant ($W_4<0$, $W_6<0$) on the (W_4,W_6) plane; if in the fourth quadrant ($W_4>0, W_6<0$), it is "hcp" (an open square). Analogously, a particle with $N_c=14$ is identified as "bcc" (a solid square) if in the first quadrant ($W_4>0$, $W_6>0$). For those particles with $N_c=13$, we extend the calculations of W_4 and W_6 into the reassembled clusters with "$N_c=12$ or 14" as mentioned earlier; "fcc" (a shaded triangle), "hcp" (an open triangle), and "bcc" (a solid triangle) are then assigned according to the signs of W_4 and W_6 as in the preceding cases. A cross designates a particle which has both the bcc and the fcc-hcp characterizations. An open circle indicates a particle which does not belong to any of the characterizations mentioned above. We here observe a substantial degree of polycrystalline nucleations of localized fcc and hcp structures, another indication of a glass state.

As Fig. 11 shows, $G_6(r)\simeq 0.2$ over the entire MC-cell volume in the metastable state. This value is to be compared with $G_6(r)\simeq 0.25$ in the bcc-lattice simulation and $G_6(r)\simeq 0$ in the fluid simulation, both in Fig. 4. A long-range bond-orientational symmetry thus appears to be established in the metastable state, a further indication of a glass state. The values of $G_4(r)$, on the other hand, stay around zero in this metastable state, as in the cases of Fig. 4.

B. Gradual quench to $\Gamma=400$

In Fig. 12 we plot $g(r)$ obtained at two different stages of evolution, $c=50$ and 80, both apparently in the metastable state. The peaks in $g(r)$, however, do not correspond exactly to either the fcc-hcp or the bcc crystalline peaks.

Figure 13 shows the sequential evolutions of Q_4 and Q_6, with the metastable values approximately 0.06 and

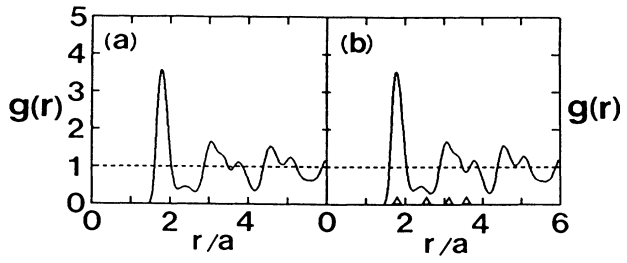

FIG. 12. Same as Fig. 6, but for the gradual quench (B) to $\Gamma=400$: (a) at $c=50$ and (b) at $c=80$.

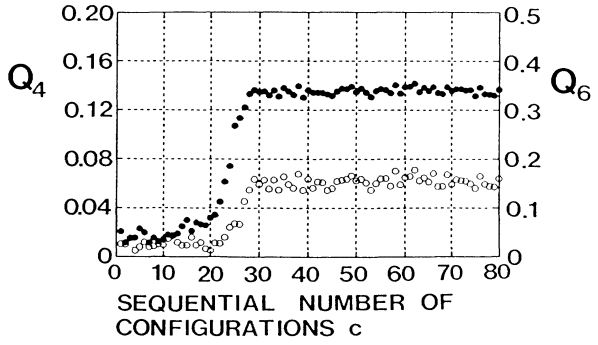

FIG. 13. Same as Fig. 7, but for the gradual quench (B) to $\Gamma=400$.

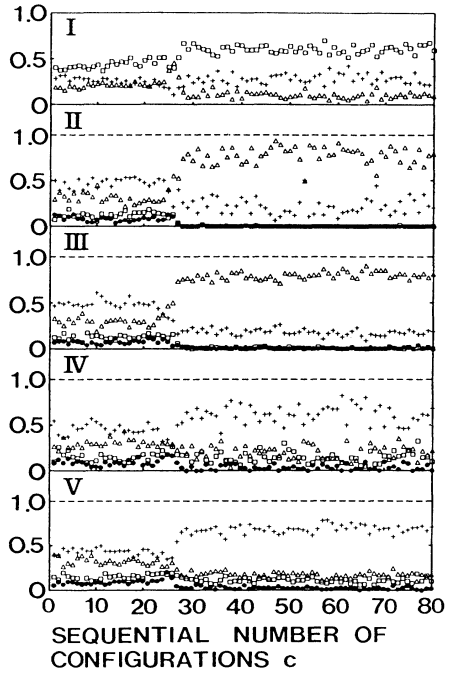

FIG. 14. Same as Fig. 8, but for the gradual quench (B) to $\Gamma=400$.

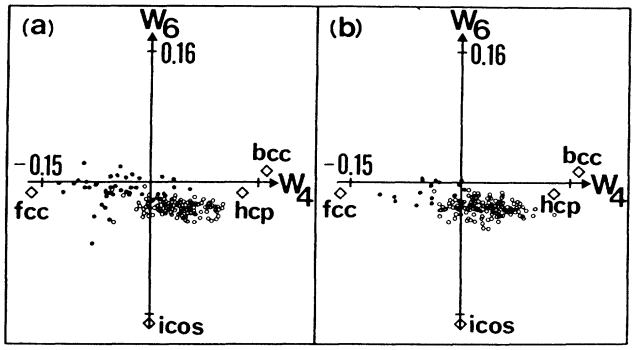

FIG. 15. Same as Fig. 9, but for the gradual quench (B) to $\Gamma=400$: (a) at $c=50$ and (b) at $c=80$.

0.35. The latter implies the existence of a bond-orientational symmetry over the entire MC cell.

In Fig. 14I, we find that the fractional numbers of particles with $N_c=12$, 13, and 14 are 0.3, 0.6, and 0.1, respectively, in the metastable state; these values are almost the same as those in the sudden quench (A) (Fig. 8).

Two-dimensional (W_4, W_6) maps in Fig. 15 show features rather different from those in the sudden quench (A). The distribution of W_6 values appears to imply a substantial involvement of the local icosahedral struc-

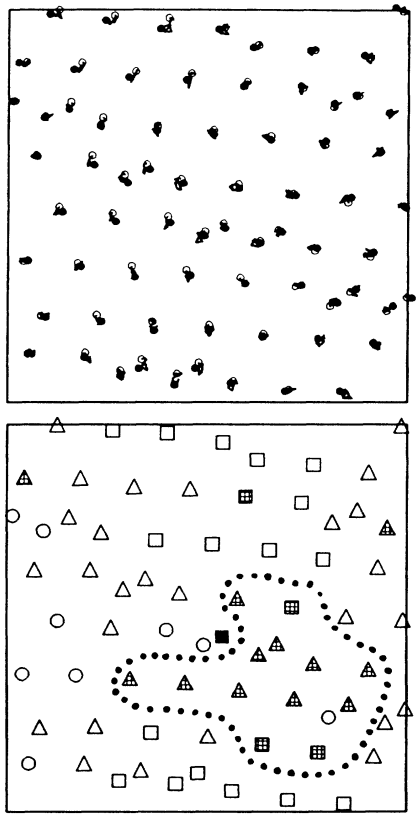

FIG. 16. Same as Fig. 9, but for the gradual quench (B) to $\Gamma=400$.

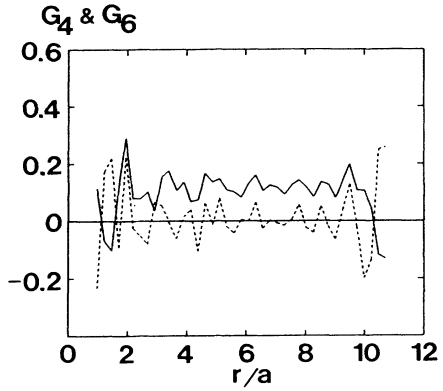

FIG. 17. Same as Fig. 11, but for the gradual quench (B) to $\Gamma=400$.

tures, although the periodic boundary conditions in the MC simulations may limit emergence of a perfect icosahedral structure. We find that a large fraction of the particles tend to form hcp clusters while bcc clusters are rare. These features are seen also in the sequential-evolution diagrams of Figs. 14II–V.

Two-dimensional (x,y) mappings of the MC particles within the thickness $\Delta z=2a$ in the metastable state, shown in Fig. 16, indicate that the particles are virtually locked around their own equilibrium positions and that the long-range translational order is apparently impaired in the equilibrium positions; nucleations of localized fcc and hcp structures are detected in this glass state. Analogously to the case of sudden quench (A), we find in Fig. 17 that an extended bond-orientational symmetry exists in the metastable state, since $G_6(r)\simeq 0.15$ over the entire MC-cell volume.

C. Sudden quench to $\Gamma=300$

The radial distribution function, shown in Fig. 18, begins with a smooth function of r at $c=5$, develops peaks reflecting the bcc crystalline structures in the plateau

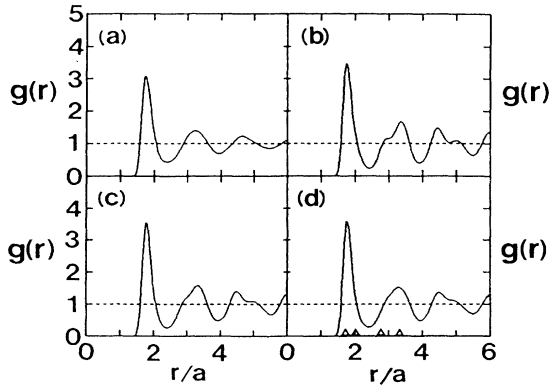

FIG. 18. Same as Fig. 6, but for the sudden quench (C) to $\Gamma=300$: (a) at $c=5$, (b) at $c=15$, (c) at $c=30$, and (d) at $c=60$. The triangular markers depict the positions of nearest-neighbor particles in the bcc structures.

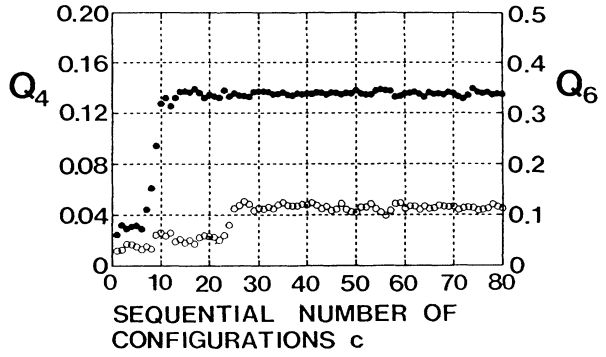

FIG. 19. Same as Fig. 7, but for the sudden quench (C) to $\Gamma=300$.

state at $c=15$, and becomes a smoother function in the metastable state at $c=30$; the state at $c=60$ remains unchanged.

In the metastable state, Fig. 19 shows that $Q_4\simeq 0.04$ and $Q_6\simeq 0.35$; these are to be compared with $Q_4\simeq 0.02$ and $Q_6\simeq 0.35$ in the plateau state. The increase of Q_4 in the metastable state may imply a decrease in the involvement of the bcc structures (see Table I).

Figure 20I shows that fractions of the clusters with $N_c=12$, 13, and 14 are 0.20, 0.35, and 0.45, respectively, in the metastable state, while 0.05, 0.35, and 0.60 in the plateau state. These again indicate predominance of the bcc structures in the plateau state and a decrease in the involvement of the bcc structures in the metastable state. At the transition from the plateau state to the metastable

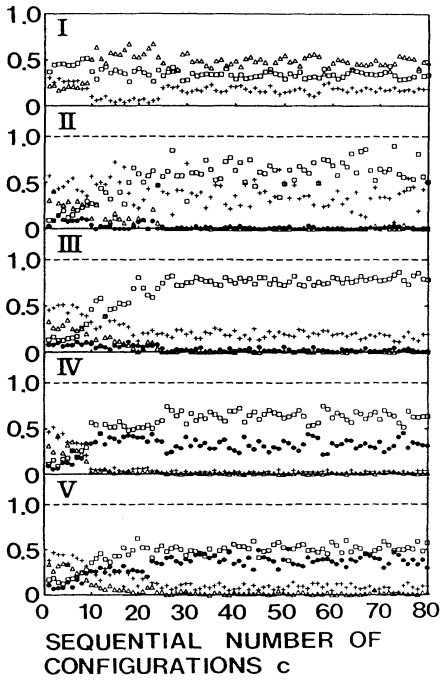

FIG. 20. Same as Fig. 8, but for the sudden quench (C) to $\Gamma=300$.

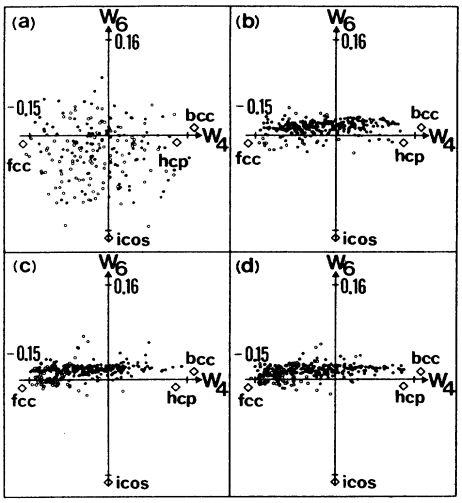

FIG. 21. Same as Fig. 9, but for the sudden quench (C) to $\Gamma=300$: (a) at $c=5$; (b) at $c=15$; (c) at $c=30$; and (d) at $c=60$.

state around $c=24$, the fraction of the fcc clusters increases (Fig. 20II), concurrently with the decrease in that of the bcc structures (Fig. 20IV). It appears, however, that a substantial interference between the clusters with $N_c=12$ and those with $N_c=14$ are involved so that a

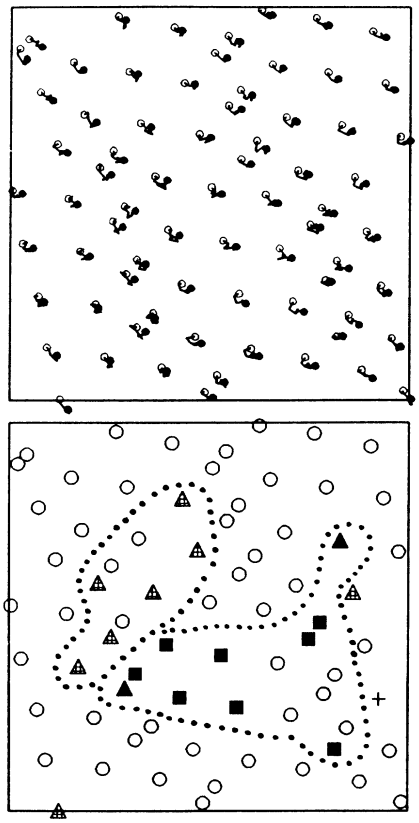

FIG. 22. Same as Fig. 10, but for the sudden quench (C) to $\Gamma=300$.

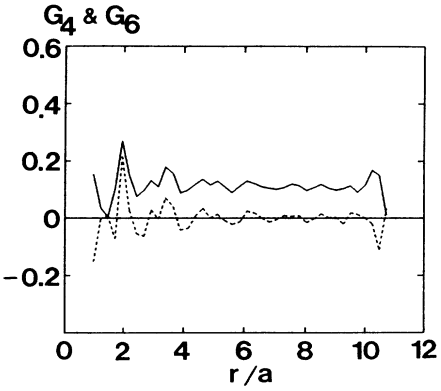

FIG. 23. Same as Fig. 11, but for the sudden quench (C) to $\Gamma=300$.

large fraction of the particles are found in the second quadrant in the metastable state These features are also exhibited in the (W_4, W_6) maps of Fig. 21 as well as in Figs. 20II–V.

Two-dimensional mappings of the real-space trajectories in the metastable state (Fig. 22) show once again that the particles are virtually locked around their own equilibrium positions and that the long-range translational order has been impaired. In this glass state we find the localized bcc structures with substantial admixtures of the localized fcc structures.

Extended bond-orientational symmetry remains in this glass state as well. Figure 23 shows that $G_6(r)\simeq 0.1$ over the entire MC-cell volume.

D. Sudden quench to $\Gamma=200$

Radial distribution functions, shown in Fig. 24, are smooth functions of r, as that in the fluid tate at $\Gamma=160$ (see Fig. 1). Figure 25 indicates that $Q_4\simeq 0.01$ and $Q_6\simeq 0.05$, slightly larger than those in the fluid state at $\Gamma=160$. Figures 26 show that either fractional numbers of particles with $N_c=12$, 13, and 14 or fractional numbers of those clusters in the four quadrants remain unchanged from those in the fluid phase at $\Gamma=160$. Particles with $N_c=12$ and 14 are widely scattered on the (W_4, W_6) maps of Fig. 27. Particles diffuse randomly from $c=20$ to $c=28$ as exhibited in Fig. 28. An extended

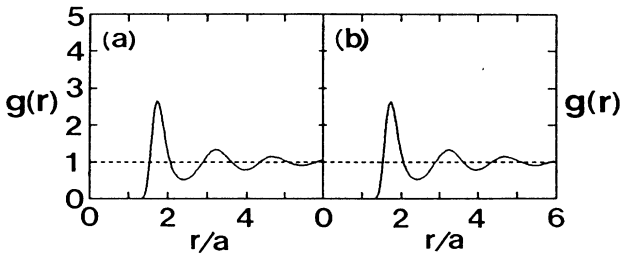

FIG. 24. Same as Fig. 6, but for the sudden quench (D) to $\Gamma=200$: (a) at $c=10$ and (b) at $c=25$.

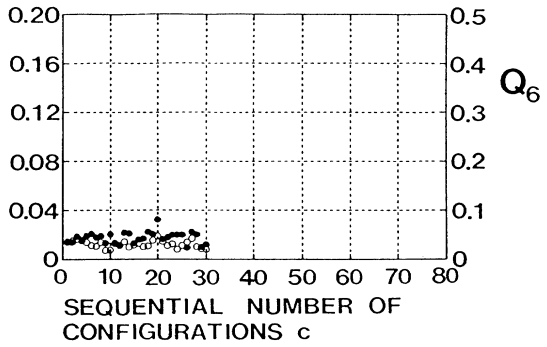

FIG. 25. Same as Fig. 7, but for the sudden quench (D) to $\Gamma=200$.

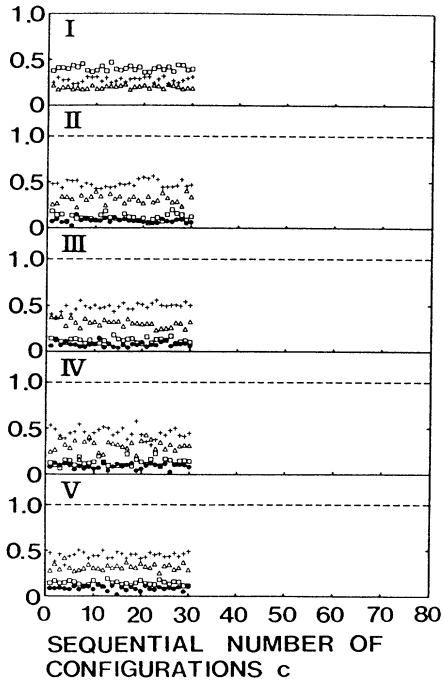

FIG. 26. Same as Fig. 8, but for the sudden quench (D) to $\Gamma=200$.

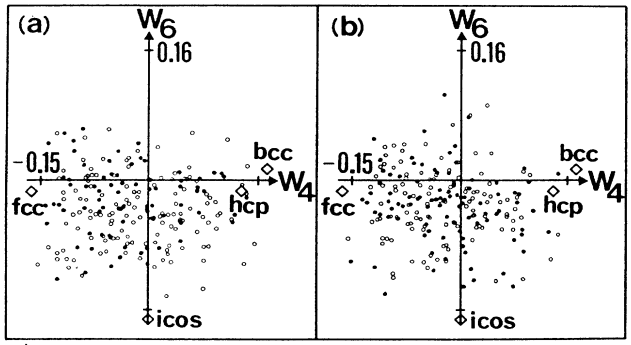

FIG. 27. Same as Fig. 9, but for the sudden quench (D) to $\Gamma=200$: (a) at $c=10$ and (b) at $c=25$.

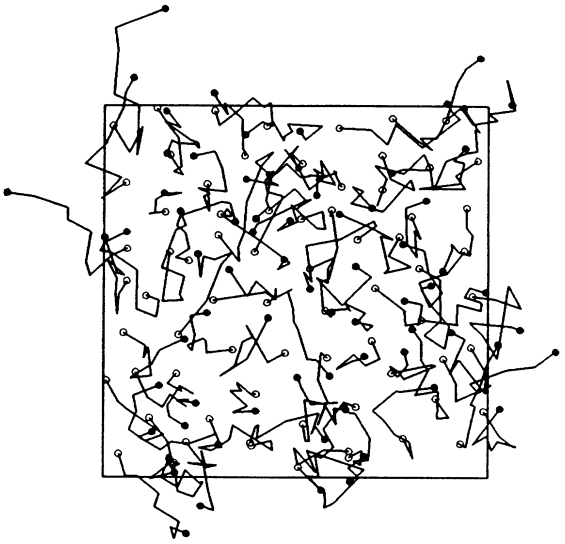

FIG. 28. Same as Fig. 10 (top), but for the sudden quench (D) to $\Gamma=200$, from the open circles at $c=20$ to the solid circles at $c=28$.

bond-orientational order does not exist in this metastable state, as Fig. 29 shows. Consequently, the state realized in this quench is a supercooled fluid state, and not a glass.

The normalized diffusion coefficient in this supercooled fluid state can be calculated with the aid of Eq. (5) as $D^* \equiv \langle (\Delta r/a)^2 \rangle / 6\omega_p t = 0.0057$. This value is about a quarter of the one derived from an extrapolation of the diffusion coefficient formula, $D^* = 2.95\Gamma^{-1.34}$, which was derived by Hansen *et al.*[13] though the MD method and is applicable for $\Gamma \leq 152.4$. This decrease in the diffusion coefficient may be interpreted as a precursor to the glass transitions, which we observed in the quenches (A), (B), and (C).

VI. DISCUSSION AND CONCLUDING REMARKS

Through examination and analyses of the MC simulation data as evidenced in the preceding section, we may

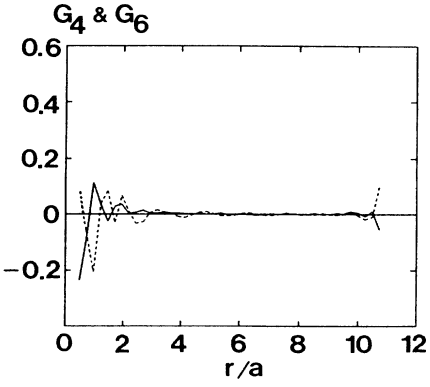

FIG. 29. Same as Fig. 11, but for the sudden quench (D) to $\Gamma=200$ at $c=20$.

conclude that the Coulomb glasses have been realized in rapidly quenched OCP's and that the glass-transition temperature corresponds to $200<\Gamma_g<300$. The polycrystalline structures of the resulting glasses depend sensitively on how the quench is applied.

In the present series of the MC simulations, we have fixed the number of the particles at $N=2\times 6^3=432$, a number appropriate to the bcc lattice. Nevertheless, the supercooled OCP's have not resulted in a pure bcc crystalline state in equilibrium; rather they have formed glasses with polycrystalline structures. We point out two reasons for these behaviors.

One is that the quenching rates are extremely rapid in all the four cases of the present simulations. The correspondence (5) tells us that even in the case of the "gradual quench" (B), the temperature has decreased by a factor of $\frac{1}{2.5}$ during a span of $6.2\times 10^3\omega_p t$.

Another reason may be traced to the closeness of the Madelung energies among the fcc, hcp, and bcc structures in the Coulomb lattice. Specifically we note the Madelung energies

$$\frac{E}{Nk_BT}=\begin{cases}-0.895\,929\Gamma & (\text{bcc})\\ -0.895\,874\Gamma & (\text{fcc})\\ -0.895\,838\Gamma & (\text{hcp}),\end{cases} \tag{12}$$

so that at $\Gamma=400$

$$\frac{E_{\text{fcc}}-E_{\text{bcc}}}{Nk_BT}=0.022\ ,$$

$$\frac{E_{\text{hcp}}-E_{\text{bcc}}}{Nk_BT}=0.036\ .$$

Those values are in fact comparable to the standard deviations of the excess internal energies averaged over 0.1 (cf. Fig. 5). Thermal fluctuations and transitions between different cluster structures appear quite probable.

To achieve an equilibrated state with a clear distinction between different cluster structures, a truly gradual quench to a temperature much lower than $\Gamma=400$ appears necessary; work in these directions is in progress.

ACKNOWLEDGMENTS

We wish to thank Dr. Y. Hiwatari, Dr. S. Nosé, and Dr. M. Tanaka for useful discussions. This research was supported in part though Grants-in-Aid for Scientific Research provided by the Japanese Ministry of Education, Science, and Culture. Computations were performed on a HITAC M-68XH/S-810 model 20 supercomputer system at the Computer Center of the University of Tokyo.

[1]B. J. Alder and T. E. Wainwright, J. Chem. Phys. **33**, 1439 (1960).
[2]J. M. Gorden, J. H. Gibbs, and P. D. Fleming, J. Chem. Phys. **65**, 2771 (1976).
[3]S. Nosé and F. Yonezawa, J. Chem. Phys. **84**, 1803 (1986); Solid State Commun. **56**, 1009 (1985).
[4]S. Nosé and F. Yonezawa, Solid State Commun. **56**, 1005 (1985).
[5]M. Tanemura, Y. Hiwatari, H. Matsuda, T. Ogawa, N. Ogita, and A. Ueda, Prog. Theor. Phys. **58**, 1079 (1977); **59**, 606 (1978).
[6]J. N. Cape and L. V. Woodcock, J. Chem. Phys. **72**, 976 (1980).
[7]S. Ichimaru, Rev. Mod. Phys. **54**, 1017 (1982).
[8]W. L. Slattery, G. D. Doolen, and H. E. DeWitt, Phys. Rev. A **26**, 2255 (1982).
[9]S. Ogata and S. Ichimaru, Phys. Rev. A **36**, 5451 (1987).
[10]H. C. Andersen, J. Chem. Phys. **72**, 2384 (1980).
[11]S. Nosé, Mol. Phys. **52**, 255 (1984); J. Chem. Phys. **81**, 511 (1984).
[12]S. Ogata and S. Ichimaru, Phys. Rev. **38**, 1457 (1988).
[13]J.-P. Hansen, I. R. McDonald, and E. L. Pollock, Phys. Rev. A **11**, 1025 (1975).
[14]P. J. Steinhardt, D. R. Nelson, and M. Ronchetti, Phys. Rev. B **28**, 784 (1983).
[15]S. Nosé and F. Yonezawa, J. Chem. Phys. **84**, 1803 (1986).